JOC The Journal of Organic Chemistry

Article

pubs.acs.org/joc

Theoretical Studies on Palladium-Mediated Enantioselective C−H Iodination

Mei-Juan Zhou, Ti-Long Yang, and Li Dang*

Department of Chemistry, South University of Science and Technology of China, Shenzhen 518055, People's Republic of China

Supporting Information

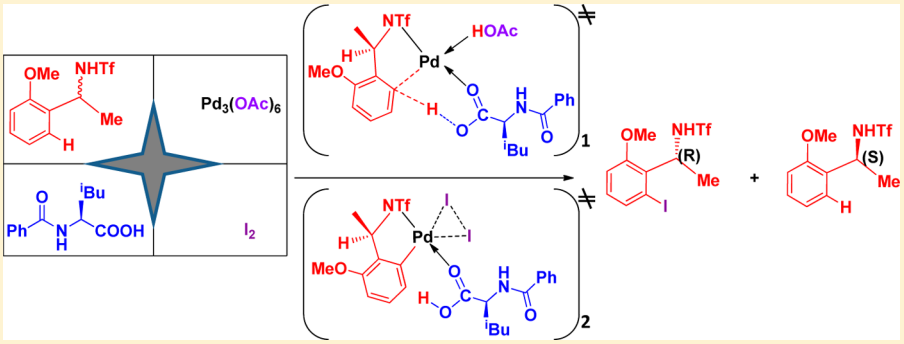

ABSTRACT: DFT calculations have been carried out to investigate the reaction mechanism for Pd^{II}-mediated enantioselective C−H iodination. Iodination of the aryl ortho C−H bond of benzylamines catalyzed by Pd^{II} diacetate complexes in the presence of the L-MPAA ligand experiences three main steps: first, C−H bond activation; second, oxidative addition of iodine on Pd^{II} and reductive elimination of iodobenzene; third, catalyst regeneration through ligand exchange. The C−H bond activation is found to be the rate-determining step of the overall iodination due to higher activation energy. The reaction barrier for the formation of iodinated (*R*)-benzylamine is lower than that of (*S*)-benzylamine, which confirms the *R* enantioselectivity in iodination at room temperature. The retainment of the coordination of one acetic acid on Pd^{II} and the chelating MPAA ligand during the catalyzed reaction are suggested to give space economy to facilitate the C−H bond activation. The NHTf functional group on the substrate is found to be very important for ortho C−H iodination at ambient condition. Our calculated results are consistent with the experimental observations.

INTRODUCTION

The achievement of enantioselective C−H activation is significant in organic synthesis, and understanding the reaction mechanism has promoted development in this research area. Asymmetric transformations via C−H bond activation have been developed to obtain diversely useful chiral products with high levels of enantiocontrol methods.[1] The enantioselectivity of chiral carbon is often related to the reaction conditions: for instance, using a chiral catalyst to transform a prochiral C−H bond. The development of chiral ligands in transition-metal complexes to catalyze enantioselective reactions has caused a great storm in asymmetric syntheses[2] and pharmaceuticals.[3] Simple and easily available ligands with high efficiency and selectivity are becoming more and more attractive. Readily available amino acid ligands as enantiomerically pure chiral compounds with two coordination sites have played an important role in enantioselective syntheses.[4] Among the chiral amino acid ligands, chiral mono-N-protected amino acid (MPAA) ligands in high-valent palladium complexes have led to efficient,[5] high-selectivity[6] and high-yield[7] C−H activations for a wide scope of substrates.[8,9] Importantly, high enantioselectivity achieved by using MPAA ligands[10] in Pd^{II} catalysts to activate meta-C−H bonds in phenyl group with long distance nitriles and ethers as donating groups was reported by Yu et al.[11] and studied theoretically by Wu et al.[12] In addition, the protecting group amine-trifluoromethylsulfonamide[13] (NHTf) in the substrate was found to be necessary for high yield and ee, especially for the ortho C−H bond activation.[13a]

Recently, Yu et al.[14] also reported the palladium-catalyzed ortho C−H iodination of racemic benzylamine substrates with enantioselectivities of up to 244 at room temperature in kinetic resolution, in the presence of MPAA (Bz-Leu-OH) ligands and the trifluoromethylsulfonamide (NHTf) protecting group at

Scheme 1. Enantioselective C−H Iodination of Benzylamine[14]

Received: November 8, 2015
Published: January 12, 2016

DOI: 10.1021/acs.joc.5b02571
J. Org. Chem. 2016, 81, 1006−1020

Chart 1. Energy Changes of Equations 1−3

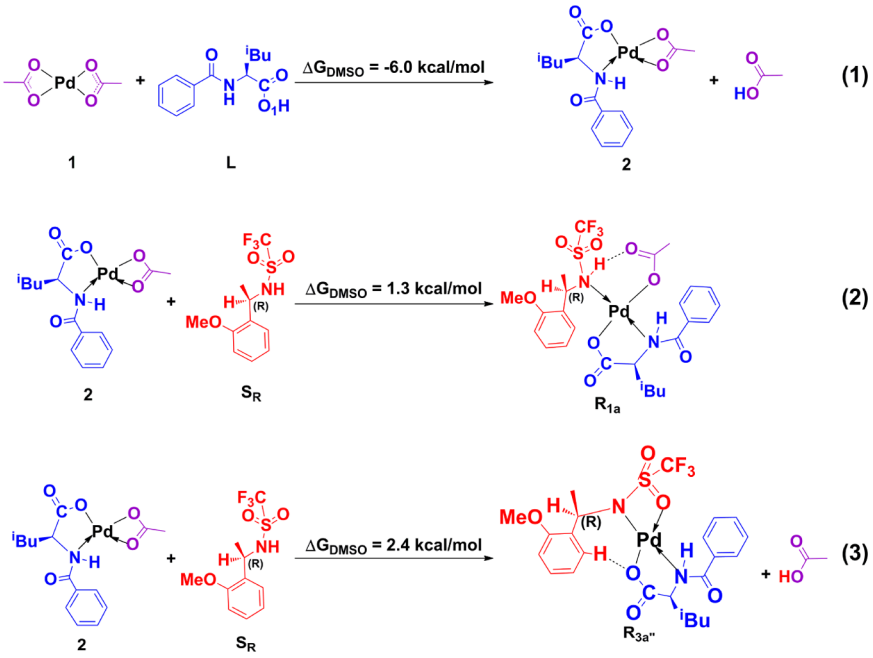

Scheme 2. Proposed Reaction Steps for the Kinetic Resolution Iodination of Benzylamine

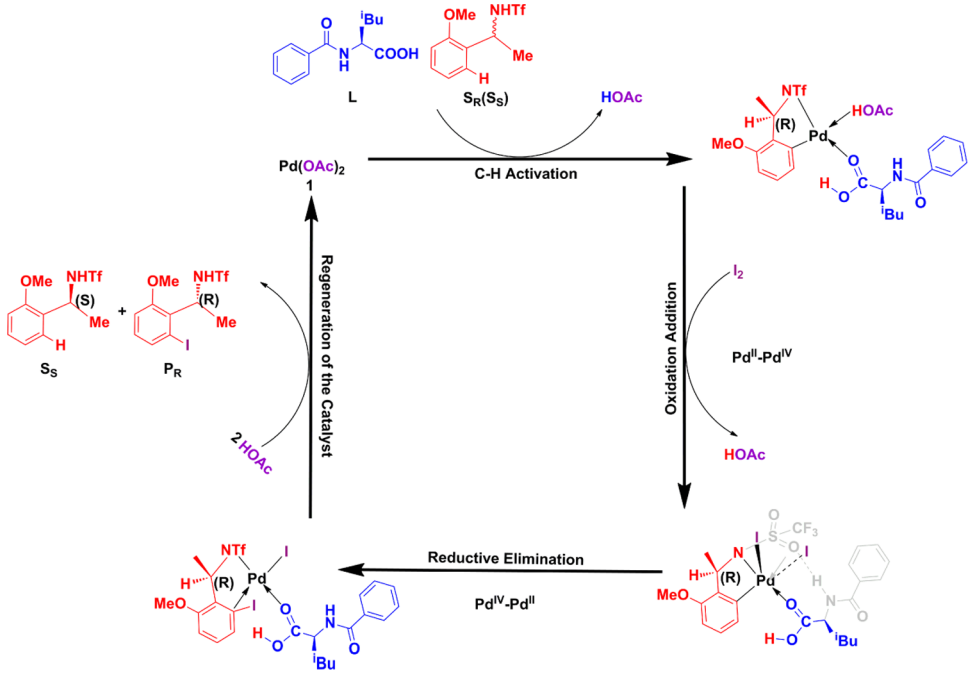

the substrate (Scheme 1). This high selectivity for the *R* configuration in the product caused our great interest. Although many people have explained the kinetic resolution of chiral amines by using models with DFT calculations,[15] and an early view has suggested that the reaction proceeds through a deprotonation from the internal nitrogen protecting group rather than an outer-sphere base,[16] a complete theoretical study on the mechanism of C−H iodination for (*R*)- and (*S*)-benzylamines (PhC*HRNHTf, Tf = trifluoromethylsulfonamide, R = Ar, alkyl) together with the kinetic enantioselectivity has not been seen. On the basis of previous studies,[11,12,14] we performed computational studies to get insight into the regioselectivity and kinetic enatioselectivity of this tremendous reaction. The role of the MPAA ligand and trifluoromethylsulfonamide (NHTf) substituent in the substrate for Pd-catalyzed aryl C−H iodination is also addressed in this work.

COMPUTATIONAL DETAILS

In this article, all of the configurations were optimized at the B3LYP[17]/{Lanl2dz+f for Pd and I and 6-31G(d) for other atoms} level of theory of the Gaussian 09 software package[18] without any symmetry constraint at the gas phase (T = 298.15 K), and the single-point energies were calculated with M06[19]/(Lanl2dz+f for Pd and I and 6-311++G(d, p) for others) based on the gas-phase optimized geometry. The solvent correction was calculated with the IEFPCM solvation

DOI: 10.1021/acs.joc.5b02571
J. Org. Chem. 2016, 81, 1006−1020

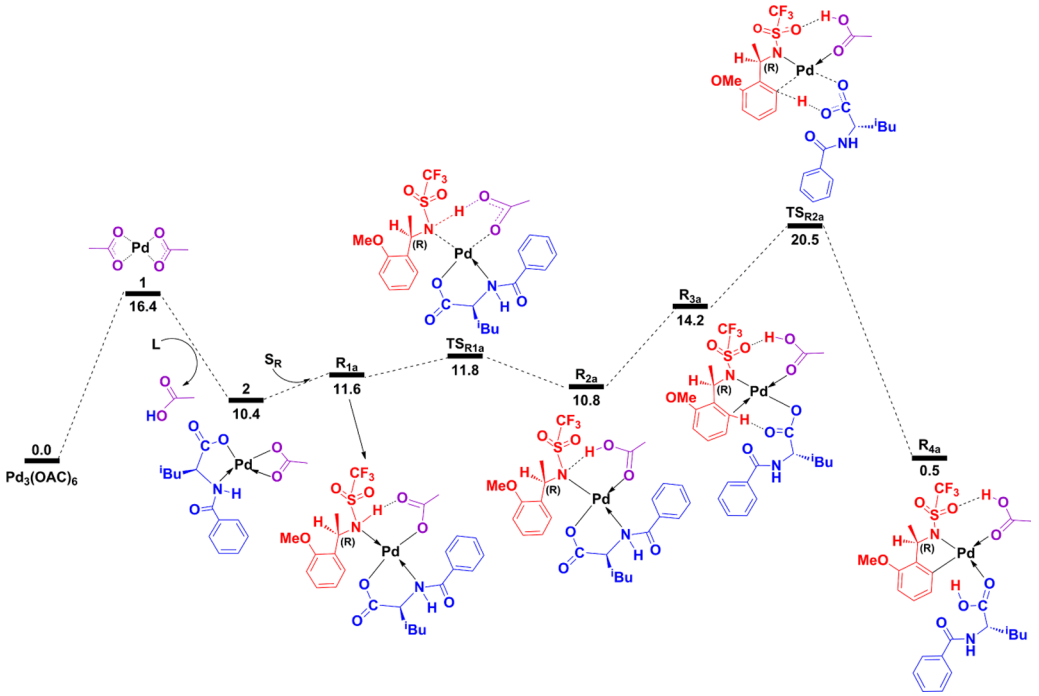

Figure 1. Energy profile of pathway a for aryl C−H bond activation of (*R*)-benzylamine. The relative free energies in dimethyl sulfoxide (DMSO) are given in kcal/mol.

model[20] in dimethyl sulfoxide (DMSO). The most favorable C−H activation reaction pathway was also calculated by WB97XD[21] and TPSSTPSS,[22] and the results were consistent with the B3LYP calculated results (see the Supporting Information). For each intermediate and transition state, the gas-phase calculated geometry shown in this paper is the most stable one in comparison with all possible conformations for the same molecule. The harmonic vibrational frequencies of reactants and products had no imaginary frequency, and the harmonic vibrational frequencies of transition state structures had only one imaginary frequency. The transition states were also confirmed to connect appropriate intermediates, reactants, or products by intrinsic reaction coordinate (IRC) calculations.[23] The gas-phase free energies (G) were calculated at T = 298.15 K within the harmonic potential approximation at optimized structures. The 3D molecular structures displayed in this article were drawn by using the GaussView 5.0 and ChemDraw molecular visualizing and manipulating programs. All energies shown in the figures and discussed in this paper are the Gibbs free energies (ΔG_{DMSO}) in the DMSO where specified, and the relative electronic energies and free energies in the gas phase are given in tables in Supporting Information. Optimized geometries and selected structural parameters for species in energy profiles are also shown in the Supporting Information.

In order to show that the DFT method used in our calculations is appropriate, TPSS and ω-B97XD methods were also used to compute the C−H activation barriers for *R* and *S* substrates (Table S1 in the Supporting Information). The computational results from TPSS and ω-B97XD are consistent with those from B3LYP. The most favorable C−H activation barriers for (*R*)-benzylamine are calculated to be 7.3, 6.8, and 8.3 kcal/mol in energy lower than those for the *S* configuration by using B3LYP, TPSSTPSS, and ω-B97XD, respectively. These results confirm that our discussion based on the B3LYP calculated results is reasonable.

RESULTS AND DISCUSSION

In order to compare the relative coordination abilities of ligands and substrates with the palladium center, we studied the energy changes in eqs 1−3 (Chart 1). When the acetate in Pd^{II} diacetate complex **1** is protonated by the carboxyl group of the MPAA ligand to give complex **2** in eq 1, the Gibbs free energy in DMSO is reduced by 6 kcal/mol. This result shows that the Pd^{II} prefers to form a bond with the MPAA ligand rather than acetate. In eq 2, the Pd^{II} complex **2** goes on to coordinate with the substrate $\mathbf{S_R}$, which is an (*R*)-benzylamine by forming a Pd−N^2 noncovalent bond in the presence of acetate ligand, and the Gibbs free energy in DMSO is increased by 1.3 kcal/mol. However, after the protonation and release of acetate, a Pd−N^2 covalent bond is formed with a free energy increase of 2.4 kcal/mol in eq 3, which is slightly larger than that in eq 2, showing that the acetate ligand prefers to coordinate with the Pd center rather than be released from the metal center after protonation by the amine of the substrate. This result is also suitable for the *S* configuration substrate. These results give us a hint that $\mathbf{R_{1a}}$ may be a stable and very important intermediate in aryl C−H activation.

On the basis of experimental observation and the above calculations, we propose there are three reaction steps for this kinetic resolution iodination (Scheme 2): (1) C−H activation which selectively chooses (*R*)-benzylamine; (2) oxidative addition and reductive elimination to form a C−I bond; (3) regeneration of the catalyst by giving iodized (*R*)-benzylamine selectively with ligand replacement at the Pd center.

Table 1. Relative Gibbs Free Energy (ΔG_{DMSO}, in kcal/mol) in Figures S2, S4, and S6 in the Supporting Information for Aryl C−H Bond Activation of (*R*)-Benzylamine

structure	ΔG_{DMSO}	structure	ΔG_{DMSO}	structure	ΔG_{DMSO}
$Pd_3(OAc)_6$	0	$Pd_3(OAc)_6$	0	$Pd_3(OAc)_6$	0
$\mathbf{R_{3a'}}$	17.0	$\mathbf{R_{3a''}}$	12.8	$\mathbf{L_1}$	7.0
$\mathbf{TS_{R2a'}}$	30.1	$\mathbf{TS_{R2a''}}$	47.7	$\mathbf{TS_L}$	13.1
$\mathbf{R_{4a'}}$	7.8	$\mathbf{R_{4a''}}$	10.5	$\mathbf{L_2}$	11.4
				$\mathbf{R_{3b}}$	24.2
				$\mathbf{TS_{R2b}}$	37.2
				$\mathbf{R_{4b}}$	15.9

DOI: 10.1021/acs.joc.5b02571
J. Org. Chem. 2016, 81, 1006−1020

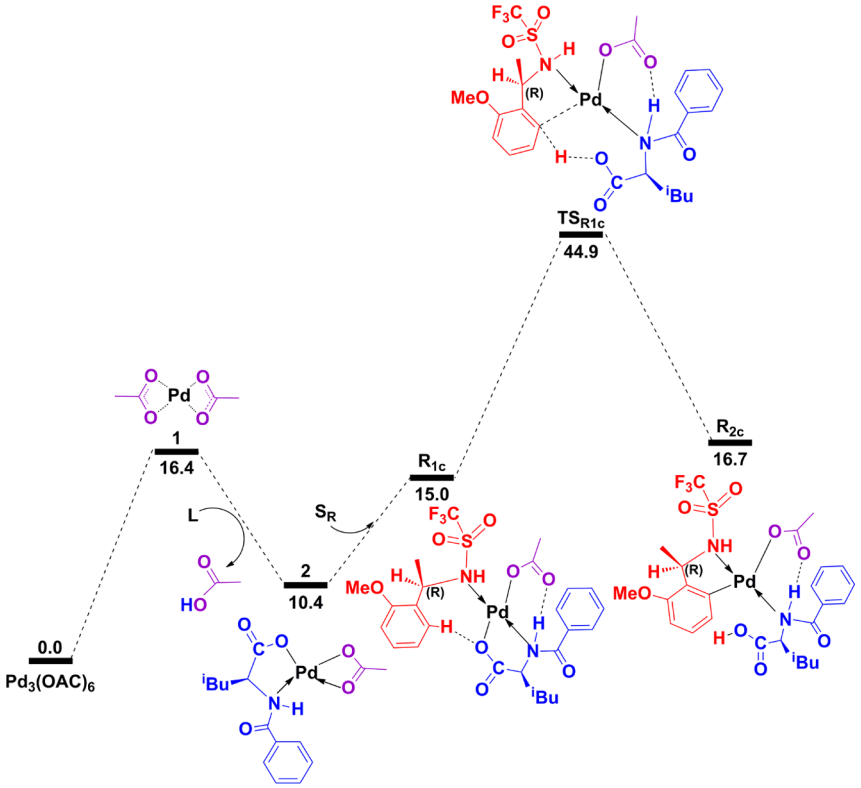

Figure 2. Energy profile of pathway c for aryl C−H bond activation of (*R*)-benzylamine. The relative free energies in dimethyl sulfoxide (DMSO) are given in kcal/mol.

The detailed reaction mechanism for *R* configuration benzylamine is studied first in this work. Previous studies have shown that $Pd(OAc)_2$ is the active species in the $[Pd_3(OAc)_6]$-catalyzed iodination of aryl C−H bonds.[12] Figure 1 shows that the monomeric $Pd(OAc)_2$ is more unstable than the trinuclear complex $[Pd_3(OAc)_6]$ by 16.4 kcal/mol in the DMSO corrected free energy. Complex **2** is formed by a ligand exchange process, which is exothermic as shown in eq 1 in Chart 1. Once the *R* configuration substrate comes in to react with complex **2**, the intermediate $\mathbf{R_{1a}}$ is formed by a hydrogen bond interaction between the amine group of the substrate and acetate together with the noncovalent bond formed between the substrate and the metal center. Then the acetate ligand is protonated by the amine of the substrate and a Pd−N covalent bond is formed, which is barrierless. $\mathbf{R_{2a}}$ is more unstable than the reference complex by 10.8 and 3.4 kcal/mol energy for the isomerization from $\mathbf{R_{2a}}$ to $\mathbf{R_{3a}}$ afterward. In $\mathbf{R_{3a}}$, the carboxylate of the substrate coordinates with the metal center. The transition state $\mathbf{TS_{R2a}}$ from the isomer $\mathbf{R_{3a}}$ is located for the aryl ortho C−H bond activation with a solvent-corrected free energy of 20.5 kcal/mol. The stable intermediate $\mathbf{R_{4a}}$ with Pd−N and Pd−C covalent bonds is formed after C−H activation. The activation of aryl C−H bonds goes through a six-membered cyclopalladation transition state (Figure 1), which is consistent with previous reports.[12,24] However, acetic acid is coordinated on the metal center by a noncovalent bond during the C−H activation, which plays a key role because coordinated acetic acid can push the substrate close to the carboxylate of the MPAA ligand, making the hydrogen easy to transfer from the substrate to the MPAA ligand. This kind of transition state has not been reported in previous theoretical studies on the Pd-MPAA catalyzed aryl C−H bond activation. The optimized geometry and selected structural parameters for species in Figure 1 are shown in the Supporting Information.

The pathways for C−H activation in the absence of the coordination of CH_3COOH on the metal center are shown in Figures S2 and S4 in the Supporting Information. CH_3COOH is released from $\mathbf{R_{3a}}$, and unstable $\mathbf{R_{3a'}}$ and $\mathbf{R_{3a''}}$ are formed in Figures S2 and S4 followed by the even more unstable transition states $\mathbf{TS_{R2a'}}$ and $\mathbf{TS_{R2a''}}$. The energy barriers of C−H activation via pathways in Figures S2 and S4 (Table 1) are 9.6 and 27.2 kcal/mol higher than that in Figure 1, respectively. In these two pathways, the C^2, N^2, and O^2 atoms of $\mathbf{S_R}$ are all coordinated to the Pd^{II} center in the structures of $\mathbf{TS_{R2a'}}$ and $\mathbf{TS_{R2a''}}$ when acetic acid is absent on the metal center. Here, the activation barrier is quite high due to a greater distance between the aryl ortho C−H and the carboxylate oxygen of the MPAA ligand. In a previous study, the distance between the aryl meta C−H and the carboxylate oxygen of the MPAA ligand is also reduced due to a very large ring formed in the transition states, which can also squeeze the meta C−H close to the carboxylate of the MPAA ligand, leading to a smaller reaction barrier.[12]

The energy profile of another pathway for C−H activation with the help of the carbonyl group of the MPAA ligand in the absence of acetic acid is shown in Figure S6 in the Supporting Information. In this pathway, an intermediate with a MPAA ligand and two acetates coordinated on the Pd center is formed first from the mono Pd acetates **1**. After protons are transferred from imine and carboxylate groups of the MPAA ligand to acetates at the same time via a barrier of 13.1 kcal/mol (Table 1), an intermediate $\mathbf{L_2}$, in which two acetic acids coordinate on the Pd center with two carbonyl oxygen atoms, is formed. Then the substrate replaces two acetic acid molecules to form the intermediate $\mathbf{R_{3b}}$. From this unstable intermediate the $\mathbf{R_{3b}}$, the aryl ortho C−H bond is activated with the help of carbonyl on

DOI: 10.1021/acs.joc.5b02571
J. Org. Chem. 2016, 81, 1006−1020

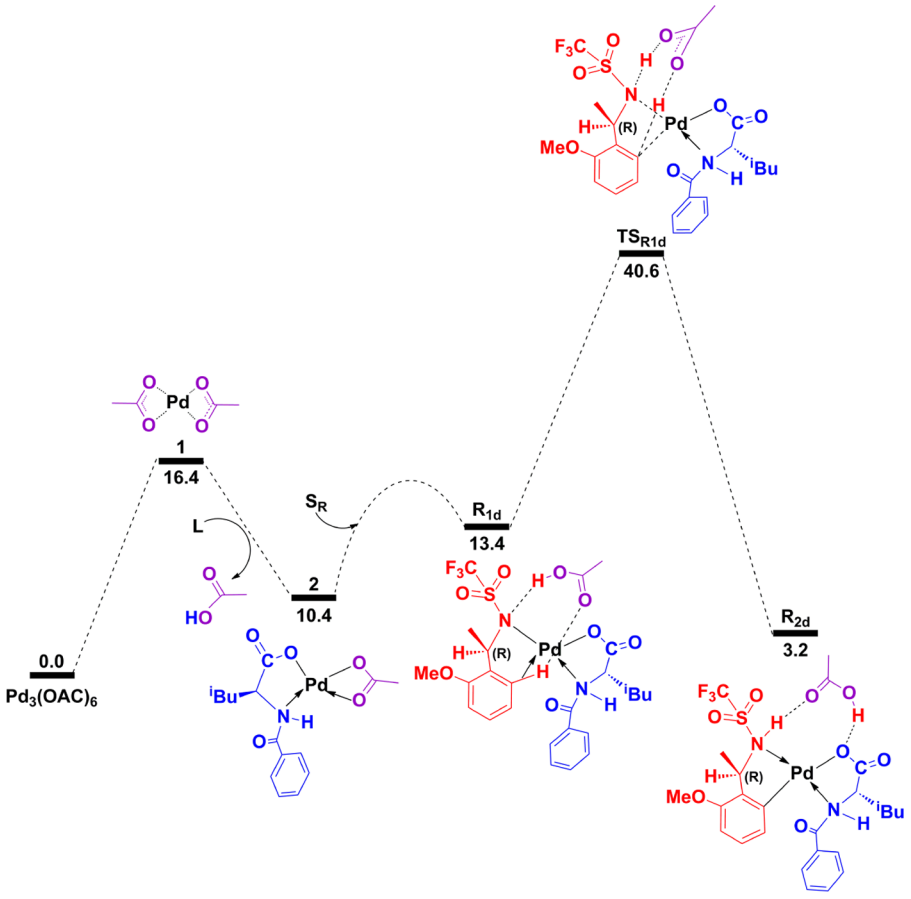

Figure 3. Energy profile of pathway d for aryl C−H bond activation of (*R*)-benzylamine. The relative free energies in dimethyl sulfoxide (DMSO) are given in kcal/mol.

the MPAA ligand through a barrier of 37.2 kcal/mol (Table 1), which is higher than that in Figure 1 by 16.7 kcal/mol. In this transition state, $\mathbf{TS_{R2b}}$, the $O^{1''}$ atom becomes a H acceptor and the Pd−N^1 noncovalent bond changes into a covalent bond, while a Pd−C^2 bond is formed so that a Pd^{II} center is kept (Figure S7 in the Supporting Information). This pathway is unfavorable because it has to pass through a very unstable intermediate, where the Pd^{II} center has two covalent bonds formed after the deprotonation of the MPAA ligand and two noncovalent bonds formed with the substrate, which moves the substrate away from the Pd^{II} center and the carboxylate group of the MPAA ligand.

Instead of formation of a hydrogen bond between the acetate and the amine group of the substrate in $\mathbf{R_{1a}}$, a hydrogen bond is formed between the acetate and imine of the MPAA ligand in $\mathbf{R_{1c}}$ in Figure 2. Without formation of a Pd−N covalent bond with N atoms in the substrate and the MPAA ligand in $\mathbf{R_{1c}}$, the activation of an ortho C−H bond is very difficult due to the very high reaction barrier of 44.9 kcal/mol, which is 24.4 kcal/mol higher than that in Figure 1. Here, $\mathbf{R_{2c}}$ is very unstable and the pathway in Figure 2 is reversible. $\mathbf{R_{1c}}$ is the isomer of $\mathbf{R_{1a}}$, the $O^{3'}$ atom of the CH_3COO fragment is H-bonded to the N^1 atom of the MPAA ligand with a 1.886 Å bond distance in the structure of $\mathbf{R_{1c}}$ (Figure S8 in the Supporting Information), and $\mathbf{R_{1c}}$ is found to be 3.4 kcal/mol higher in energy than $\mathbf{R_{1a}}$, which is consistent with the conclusion from a comparison of reaction energies of eqs 2 and 3 in Chart 1. Next, a proton transfer takes place between the C^2 atom of $\mathbf{S_R}$ and the O^1 atom of the MPAA ligand in the process of a C−H activation reaction with a higher energy barrier. $\mathbf{R_{2c}}$ is computed to be 16.2 kcal/mol higher in energy than $\mathbf{R_{4a}}$. In a word, a pathway in which only a noncovalent bond is formed between the substrate and the metal center has a higher C−H activation barrier in comparison to that in which the amine of the substrate is deprotonated and a covalent Pd−N (substrate) bond is formed; thus, the mechanism of pathway c in Figure 2 is impractical.

The pathways in Figures 3 and 4 are based on a previous study,[2d] in which the C−H activation occurred with the help of an acetic acid oxygen rather than a carboxylate oxygen of the MPAA ligand. In Figure 3, the substrate forms a Pd−N covalent bond by transferring H to acetate and $\mathbf{R_{1d}}$ is obtained, in which the aryl C−H has an agostic interaction with the Pd center. The C−H activation occurs through the transition state $\mathbf{TS_{R1d}}$, where the acetate lying above the plane of Pd^{II}−O−N forms a hydrogen bond, interacting with C^2 and N^2 of $\mathbf{S_R}$ at the same time to achieve a hydrogen transfer process (Figure S9 in the Supporting Information). However, this process has a barrier of 40.6 kcal/mol.

Similar to pathway in Figure 3, the pathway in Figure 4 has also been studied, where $\mathbf{S_R}$ coordinates to the Pd^{II} center to form $\mathbf{R_{1e}}$ on the basis of the structure of complex **3**. The C−H activation occurs through the transition state $\mathbf{TS_{R1e}}$, where the ortho C−H bond transfers H to one O of acetic acid and another O of acetic acid to form a hydrogen bond with the N of the MPAA ligand (Figure S10 in the Supporting Information). This process has a barrier of 43.3 kcal/mol (Figure 4), which is even higher than that in Figure 3. The results in these two

DOI: 10.1021/acs.joc.5b02571
J. Org. Chem. 2016, 81, 1006−1020

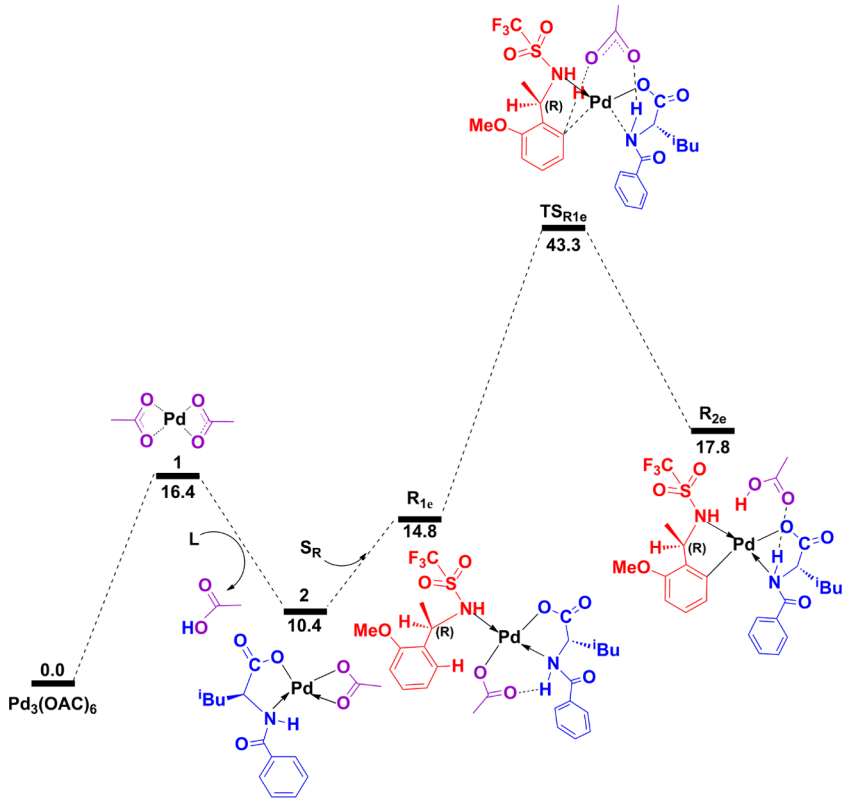

Figure 4. Energy profile of pathway e for aryl C−H bond activation of (*R*)-benzylamine. The relative free energies in dimethyl sulfoxide (DMSO) are given in kcal/mol.

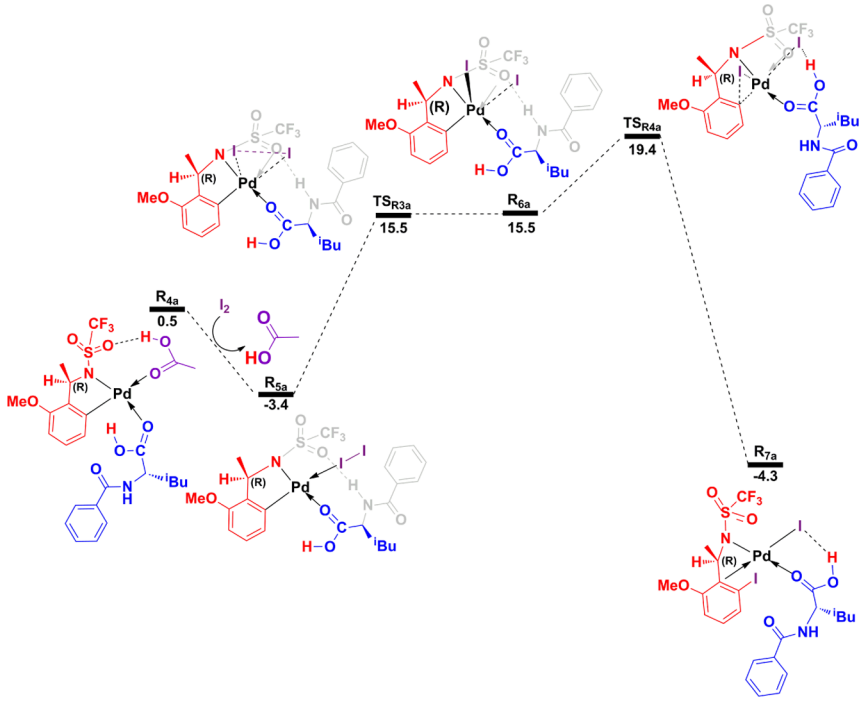

Figure 5. Energy profile for the stepwise reaction pathway of the iodination process. The relative free energies in dimethyl sulfoxide (DMSO) are given in kcal/mol.

pathways show that the ortho C−H activation prefers to occur with the carboxylate group of the MPAA ligand rather than with acetic acid due to better overlap of the meta C−H σ bond with the p orbital of the carbonyl oxygen of carboxylate of the MPAA ligand than with that of acetic acid. Up to now, the barriers in Figures S2, S4, S6 in the Supporting Information and Figures 2−4 are all higher than that in Figure 1 for C−H activation; therefore, these data could prove that the pathway in Figure 1 is the most favorable pathway and $\mathbf{R_{4a}}$ is the most stable intermediate formed after C−H activation.

DOI: 10.1021/acs.joc.5b02571
J. Org. Chem. 2016, 81, 1006−1020

Table 2. Relative Gibbs Free Energy (ΔG_{DMSO}, in kcal/mol) in Figures S12 and S14 in the Supporting Information for Metathesis Reactions of (*R*)-Benzylamine

structure	ΔG_{DMSO}	structure	ΔG_{DMSO}
$Pd_3(OAc)_6$	0	$Pd_3(OAc)_6$	0
$\mathbf{R_{5b}}$	1.9	$\mathbf{R_{5c}}$	1.7
$\mathbf{TS_{R3b}}$	29.1	$\mathbf{TS_{R3c}}$	35.8
$\mathbf{R_{6b}}$	−16.8	$\mathbf{R_{6c}}$	−2.8

Once the Pd−C bond is formed after C−H activation, the iodination of activated aryl can take place via concerted Pd−C metathesis or through a stepwise pathway with oxidative addition and reductive elimination. The stepwise pathway is shown in Figure 5, where $\mathbf{R_{5a}}$ is formed when CH_3COOH in $\mathbf{R_{4a}}$ is replaced by I_2, and the oxidative addition of I_2 occurs with a barrier of 15.5 kcal/mol while the reductive elimination goes through a barrier of 19.4 kcal/mol to form a C−I bond (Figure 5), which is lower than the C−H activation barrier in Figure 1. In Figure S11 in the Supporting Information, the amide (NHC═O) of the ligand stays away from the benzene ring of $\mathbf{S_R}$ to reduce the steric effect in the structure of $\mathbf{TS_{R4a}}$, and stable $\mathbf{R_{7a}}$ is formed afterward.

The processes of a concerted metathesis reaction for iodination have also been studied. In Figure S12 in the Supporting Information, CH_3COOH is involved during the metathesis process while CH_3COOH is coordinated to the Pd^{II} center in Figure S14 in the Supporting Information during the metathesis process. However, both barriers in Figures S12 and S14 are very high (29.1 and 35.8 kcal/mol) (Table 2), and they are higher than the total barrier in Figure 5. Thus, a concerted metathesis reaction is unfavorable in the iodination process.

The last part in the catalytic cycle is the formation of the product and regeneration of the catalyst by a protonation process. The protonation of the amine group in the substrate leads to the formation of the final product, and the protonation of the iodide regenerates the catalyst $Pd(OAc)_2$. On the basis of the sequence of protonation, there are three different pathways for this part. From the calculated results shown in Figures 6−8, we can see that the pathway in Figure 6 is the most favorable pathway, which continues from the last intermediate in Figure 5. According to this pathway, the protonation of the amine group in the substrate by CH_3COOH takes place first with a very small proton transfer barrier. Then another CH_3COOH comes in to cause protonation of iodide and the MPAA ligand and iodized benzylamine is replaced by acetate, thus regenerating $Pd(OAc)_2$. Here, 11.2 kcal/mol energy is the cost of finishing the reaction. Although these steps lead to the formation of unstable HI as the byproduct, the neutralization can reduce the energy of the system. Actually, according to Yu's report,[14] Na_2CO_3 was added into the reaction system at the end of the reaction.

Another pathway is shown in Figure 7, and the calculated structures are shown in Figure S17 in the Supporting Information. The proton transfer in this pathway happens first from the carboxylic group of MPAA to the amine group of the substrate via a 5.2 kcal/mol barrier. After this, the carboxylate in the MPAA ligand is protonated by CH_3COOH and iodide is protonated by another CH_3COOH. However, the total barrier for this protonation process is 11.4 kcal/mol, and 15.9 kcal/mol energy is the cost to form HI. In addition, the unstable HI as the byproduct can also be neutralized by base, which was added to the reaction system at the end of the reaction.

In Figure 8, an alternative reaction pathway in which ligand replacement occurs first is studied. After MPAA is replaced by CH_3COOH, the protonation of the amine group in the substrate takes place by proton transfer from CH_3COOH to the N atom in the substrate. The proton transfer needs to overcome a barrier of 13.3 kcal/mol. The proton transfer from another CH_3COOH to iodide regenerates $Pd(OAc)_2$ and forms HI. The unstable HI can be neutralized also.

The pathways in Figures 6−8 are all possible because the total energy costs in three pathways are all small and they are all

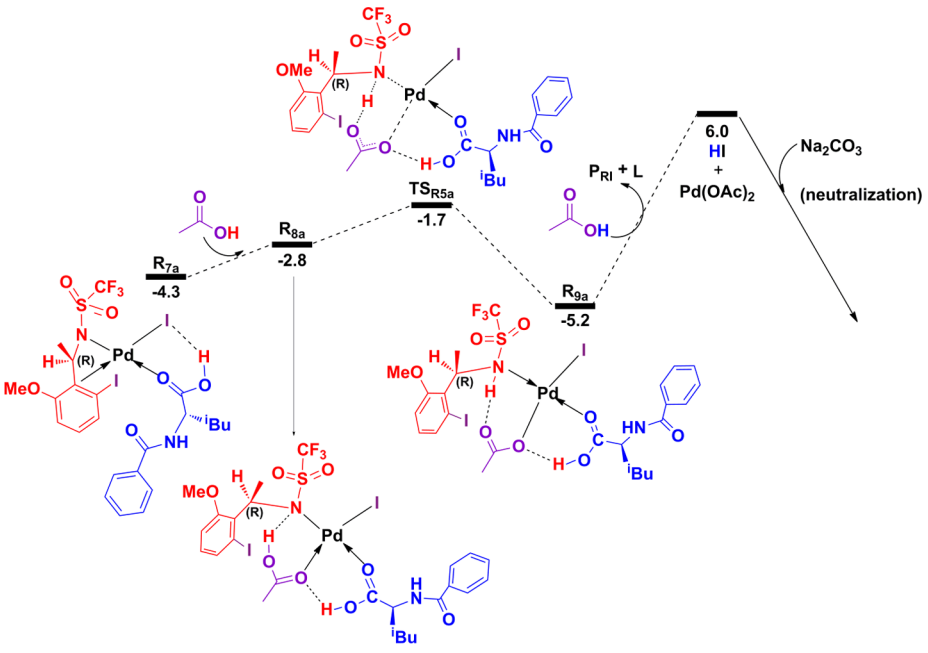

Figure 6. Energy profile of pathway a for *R*-iodinated product release and regeneration of the catalyst. The relative free energies in dimethyl sulfoxide (DMSO) are given in kcal/mol.

DOI: 10.1021/acs.joc.5b02571
J. Org. Chem. 2016, 81, 1006−1020

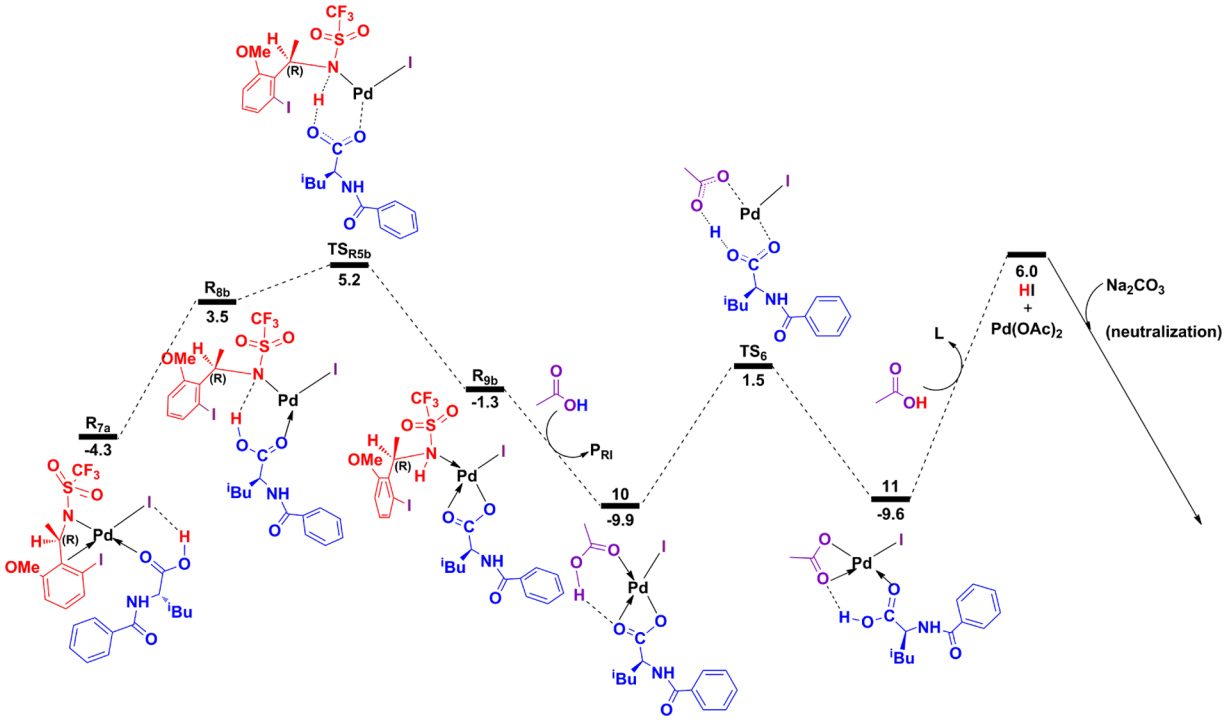

Figure 7. Energy profile of pathway b for generation of the *R*-iodinated product and the regeneration of the catalyst. The relative free energies in dimethyl sulfoxide (DMSO) are given in kcal/mol.

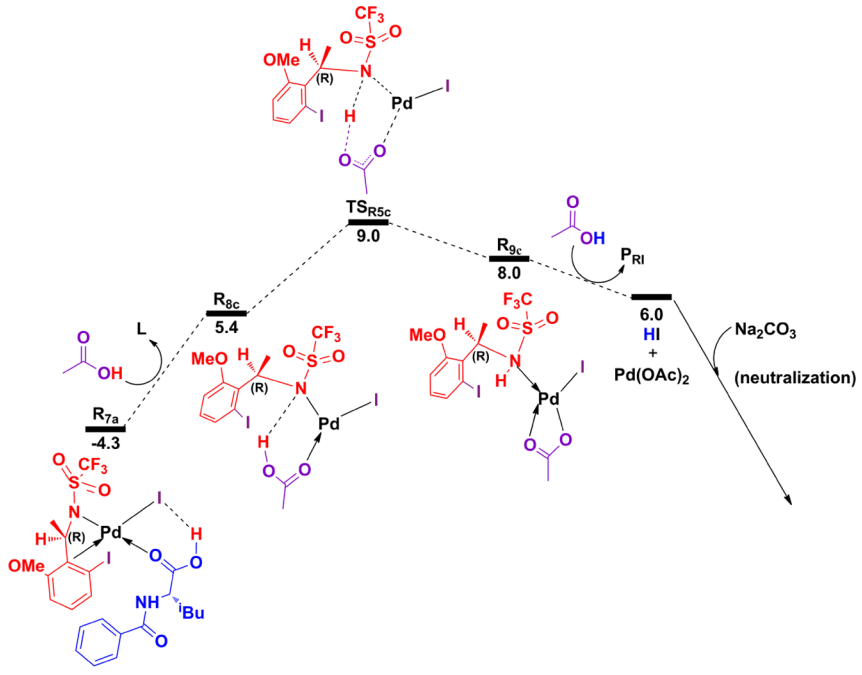

Figure 8. Energy profile of pathway c for generation of the *R*-iodinated product and the regeneration of the catalyst. The relative free energies in dimethyl sulfoxide (DMSO) are given in kcal/mol.

smaller than the C−H activation and I_2 oxidative addition and C−I reductive elimination processes, suggesting that, once the C−H activation happens, the other reaction steps are facile.

According to Yu's report,[14] the rate of fast-reaching enantiomer (k_{fast}/k_{slow}) for Pd-catalyzed C−H iodination reactions can reach up to 244 with the MPAA ligand for racemic benzylamines. We are interested in studying the detailed mechanisms for Pd-catalyzed iodation reaction processes of *S* enantiomer reagents. Similar to the reaction route for (*R*)-benzylamine ortho C−H iodination, reaction pathways for (*S*)-benzylamines are also divided into three parts, a C−H bond activation reaction and stepwise iodination including oxidative addition and reductive elimination reactions together with the regeneration of the catalyst.

First of all, the most favorable pathway for C−H activation of (*S*)-benzylamine is shown in Figure 9. Similar to that in Figure 1, **1** → **2** is a rapid reaction process, which leads to ligand replacement of the acetate by the MPAA ligand. Then the (*S*)-

DOI: 10.1021/acs.joc.5b02571
J. Org. Chem. 2016, 81, 1006−1020

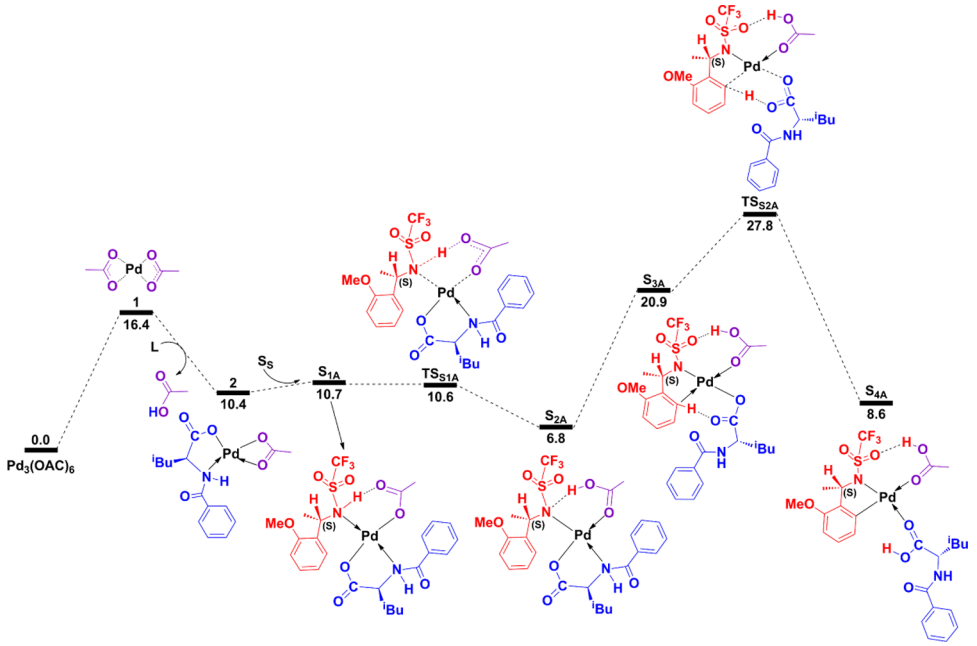

Figure 9. Energy profile of pathway A for aryl C−H bond activation of (*S*)-benzylamine. The relative free energies in dimethyl sulfoxide (DMSO) are given in kcal/mol.

Table 3. Relative Gibbs Free Energy (ΔG_{DMSO}, in kcal/mol) in Figures S20. S22, and S24 in the Supporting Information for Aryl C−H Bond Activation of (*S*)-Benzylamine

structure	ΔG_{DMSO}	structure	ΔG_{DMSO}	structure	ΔG_{DMSO}
$Pd_3(OAc)_6$	0	$Pd_3(OAc)_6$	0	$Pd_3(OAc)_6$	0
$\mathbf{S}_{3A'}$	23.4	$\mathbf{S}_{3A''}$	15.5	$\mathbf{L}_1$	7.0
$\mathbf{TS}_{S2A'}$	35.2	$\mathbf{TS}_{S2A''}$	50.5	$\mathbf{TS}_L$	13.1
$\mathbf{S}_{4A'}$	5.8	$\mathbf{S}_{4A''}$	9.3	$\mathbf{L}_2$	11.4
				$\mathbf{S}_{3B}$	30.8
				$\mathbf{TS}_{S2B}$	41.5
				$\mathbf{S}_{4B}$	14.7

benzylamine substrate coordinates with the Pd center following a deprotonation of the amine group by transferring a proton from the substrate to the remaining acetate. This deprotonation process can be promoted by the strongly electron withdrawing Tf group and nucleophilic CH_3COO^-, and the reaction barrier is 10.6 kcal/mol. Then the ortho C−H activation occurs through a barrier of 27.8 kcal/mol and the intermediate $\mathbf{S}_{4A}$ is formed. In this pathway, the total barrier is higher than that in the most favorable pathway of C−H activation for (*R*)-benzylamine by 7.3 kcal/mol.

Similar to pathways in Figures S2, S4 and S6 in the Supporting Information for (*R*)-benzyl amine, the three pathways for (*S*)-benzylamine ortho C−H activation are presented in Figures S20, S22, and S24 in the Supporting Information, respectively. In comparison with the pathway in Figure 9, the energy barriers of the pathways in Figures S20, S22, and S24 are 7.4, 22.7, and 13.7 kcal/mol higher, respectively (Table 3). In addition, the total energy barriers in the pathways in Figure 9 and Figures S20, S22, and S24 are 7.3, 5.1, 2.8, and 4.3 kcal/mol higher than those in the pathways in Figure 1 and Figures S2, S4, and S6 for (*R*)-benzylamine, respectively, suggesting that the ortho C−H bond in (*S*)-benzylamine is more difficult to activate than that in (*R*)-benzylamine. The optimized structures and selected geometric parameters of the three pathways in Figures S20, S22, and S24 are shown in Figures S21, S23, and S25 in the Supporting Information.

Another C−H activation mechanism in Figure 10 is quite similar to the pathway in Figure 2 except for (*S*)-benzylamine as the substrate. However, the total reaction barrier in this pathway is calculated to be 51.7 kcal/mol, which is 23.9 kcal/mol higher than that in pathway A and 6.8 kcal/mol higher than that in the pathway (Figure 2) of (*R*)-benzylamine. Thus, this pathway cannot compete with the pathway in Figure 9. The optimized structures and selected geometric parameters of pathway in Figure 10 is presented in Figure S26 in the Supporting Information.

Another possible pathway for C−H bond activation of (*S*)-benzylamine by taking acetic acid as a proton transfer bridge is shown in Figure 11. The amine group in the *S* substrate is first deprotonated and then protonated with proton transfer from the phenyl group to acetic acid. The total barrier for this pathway is 41.1 kcal/mol. At the same time, proton transfer from the phenyl group to acetic acid, which has a hydrogen bond with the amine of the MPAA ligand, also has a very high barrier in Figure 12. These two C−H activation pathways are all unfavorable due to very high reaction barriers in comparison with that in Figure 9.

The oxidative addition and reductive elimination reactions of (*S*)-benzylamine with the $Pd^{II-IV-II}$ mechanism also take place after the C−H activation. $\mathbf{S}_{4A}$ reacts with I_2 to form the relatively stable intermediate S_{5A} by replacing CH_3COOH with I_2. I_2 has a weak interaction with O^2 of $\mathbf{S}_S$ rather than coordinates to the Pd^{II} center in the structure of S_{5A} (Figure 13). The oxidative addition occurs with a barrier of 18.2 kcal/mol in free energy, followed by a reductive elimination to form a C−I bond as in $\mathbf{S}_{7A}$ via a 23.2 kcal/mol barrier. Here, S_{6A} is relatively more unstable than $\mathbf{TS}_{S3A}$ in solvent-corrected free energy because of the overestimation of solvent effects in $\mathbf{S}_{6A}$, since $\mathbf{S}_{6A}$ is relatively more stable than in the $\mathbf{TS}_{S3A}$ gas phase. $\mathbf{TS}_{S3A}$ is a transition state, and its structure is more flexible than that of $\mathbf{S}_{6A}$; thus, the solvent effect on $\mathbf{TS}_{S3A}$ is smaller. The

DOI: 10.1021/acs.joc.5b02571
J. Org. Chem. 2016, 81, 1006−1020

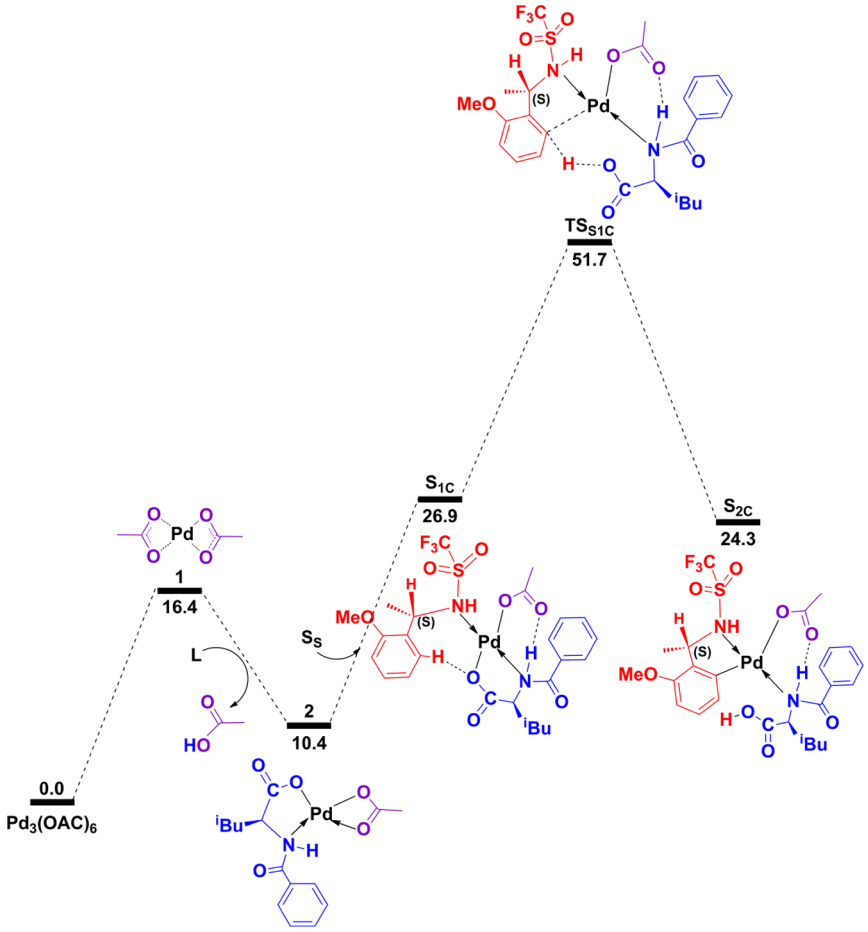

Figure 10. Energy profile of pathway C for aryl C−H bond activation of (*S*)-benzylamine. The relative free energies in dimethyl sulfoxide (DMSO) are given in kcal/mol.

optimized structures and selected geometric parameters of the pathway in Figure 13 are shown in Figure S29 in the Supporting Information. The oxidative addition and reductive elimination processes of $\mathbf{S_S}$ are similar to those of $\mathbf{S_R}$, and they are all ready to happen once the C−H activation is achieved.

The formation of a C−I bond through a metathesis reaction has also been studied for (*S*)-benzylamine (Figures S30 and S32 in the Supporting Information). However, the energy barriers of two pathways for Pd−C bond metathesis with I_2 are 16.3 and 18.6 kcal/mol higher than that of the oxidative addition and reductive elimination of (*S*)-benzylamine in Figure 13. $\mathbf{TS_{S3B}}$ is calculated to be 39.5 kcal/mol with one imaginary frequency of 111.54*i* cm^{-1} (Table 4) and is energetically 10.4 kcal/mol higher than $\mathbf{TS_{R3b}}$ (Figure S30), and $\mathbf{TS_{S3C}}$ is calculated to be 41.8 kcal/mol with one imaginary frequency of 115.07*i* cm^{-1} (Table 4) and is energetically 6.0 kcal/mol higher than $\mathbf{TS_{R3c}}$ (Figure S32). The optimized structures and selected geometric parameters in the processes of $\mathbf{S_{5B}} \rightarrow \mathbf{S_{6B}}$ and $\mathbf{S_{5C}} \rightarrow \mathbf{S_{6C}}$ are shown in Figures S31 and S33 in the Supporting Information. From an energetic standpoint, much more energy is needed to complete the formation of C^2−I^5 bond in the metathesis processes in comparison to the energy needed for the oxidative addition and reductive elimination processes. Therefore, the ortho C−Pd bond metathesis with I_2 is not favorable for either (*R*)- or (*S*)-benzylamine.

The pathways in Figures 13 and Figures S30 and S32 in the Supporting Information have been investigated similarly to the aforementioned pathways in Figure 5 and Figures S12 and S14 in the Supporting Information of $\mathbf{S_R}$. The relative Gibbs free energies (ΔG_{DMSO}) in the DMSO of pathways in Figure 13 and Figures S30 and S32 for generation of the *S*-iodinated product and the regeneration of the catalyst are summarized in Table 5. The pathway in Figure 13 is slightly more favorable than the pathways in Figures S30 and S32, since pathway A in Figure 13 is barrierless in our calculation. The mechanisms of regeneration of the catalyst are presented in Figures S34, S36, and S38 in the Supporting Information. In Figure S36, without the coordination of CH_3COOH, the proton transfer from the carboxyl of the MPAA ligand to the amine group of $\mathbf{S_S}$ occurs via a barrier of 5.8 kcal/mol. Then CH_3COOH is coordinated to the Pd^{II} center for the protonation of MPAA and iodide. After these two protonation processes, HI is formed. In addition, neutralization can drive the reaction to a low energy. The reaction barrier in Figure S38 is higher than that in Figure S34 by 11.6 kcal/mol. Now we can see that these three pathways for regeneration of the catalyst by protonation of benzylamine, MPAA ligand, and iodide around the metal center are all possible due to small reaction barriers. The optimized structures and selected geometric parameters of the pathways in Figures S34, S36, and S38 are shown in Figures S35, S37, and S39 in the Supporting Information.

Our computational study shows that ortho C−H activation of (*R*)-benzylamine has a lower barrier than ortho C−H activation of (*S*)-benzylamine, and the acetic acid coordinated to metal center catalyzes the C−H bond activation more easily

DOI: 10.1021/acs.joc.5b02571
J. Org. Chem. 2016, 81, 1006−1020

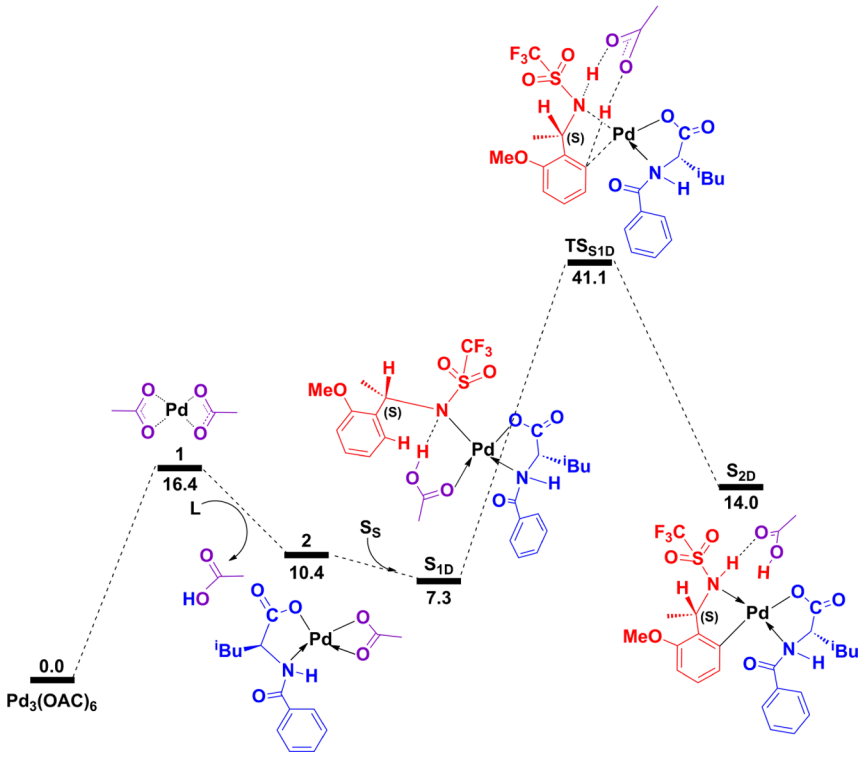

Figure 11. Energy profile of pathway D for aryl C−H bond activation of (*S*)-benzylamine. The relative free energies in dimethyl sulfoxide (DMSO) are given in kcal/mol.

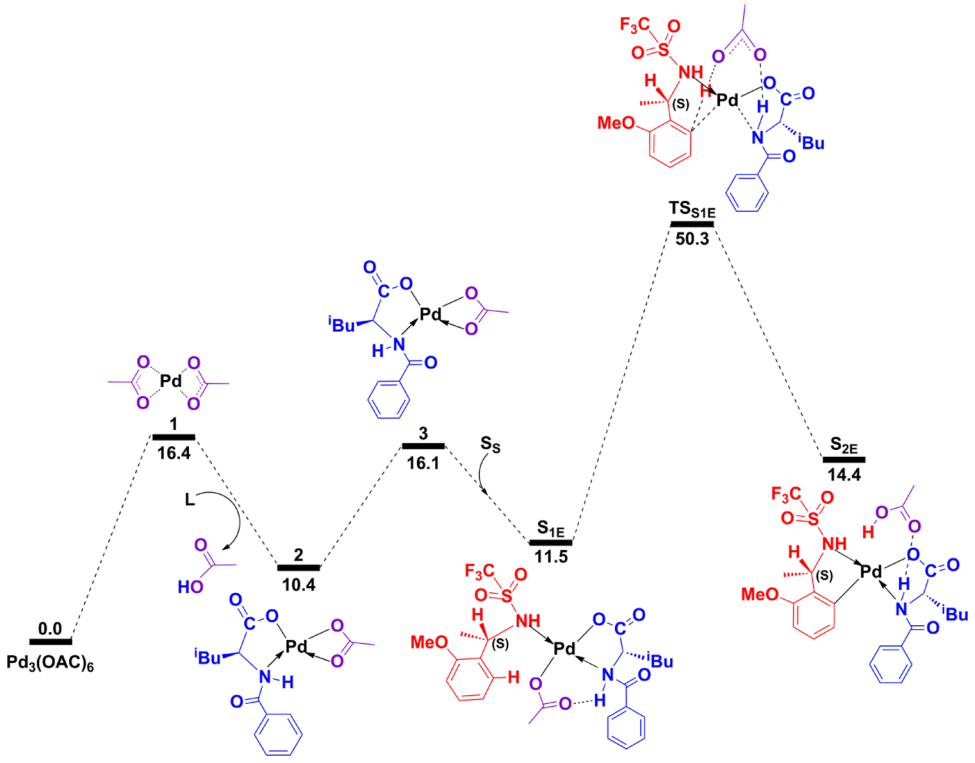

Figure 12. Energy profile of pathway E for aryl C−H bond activation of (*S*)-benzylamine. The relative free energies in dimethyl sulfoxide (DMSO) are given in kcal/mol.

than the metal center without coordination of acetic acid (Scheme 3). In the most favorable transition states (**TS$_{R2a}$** and **TS$_{S2A}$**), the rigid N−Pd−C angle leaves space for the acetic acid to coordinate to the Pd center and it is the space permission which in turn makes the ortho C−H closer to the carboxylate of the MPAA ligand to facilitate the proton transfer. This conclusion induces conjecture about DMSO, which can have a similar effect on C−H activation to acetic acid. We have carried

DOI: 10.1021/acs.joc.5b02571
J. Org. Chem. 2016, 81, 1006−1020

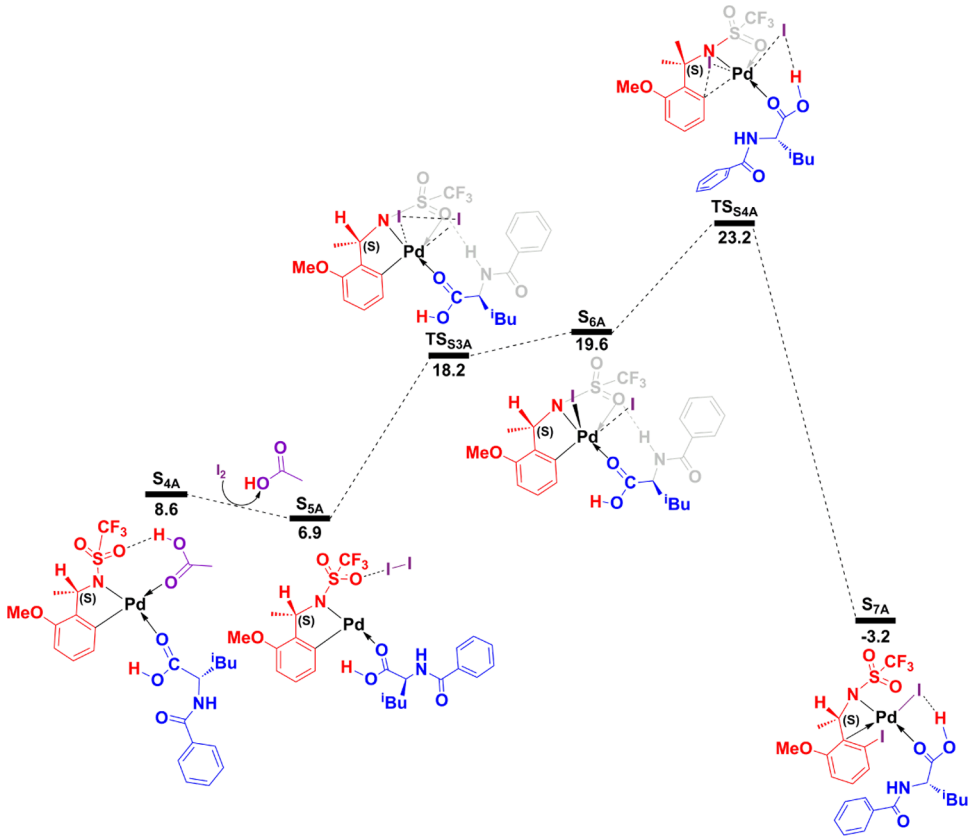

Figure 13. Energy profile for the iodination reaction of (*S*)-benzylamine. The relative free energies in dimethyl sulfoxide (DMSO) are given in kcal/mol.

Table 4. Relative Gibbs Free Energy (ΔG_{DMSO}, in kcal/mol) in Figures S30 and S32 in the Supporting Information for Metathesis Reactions of (*S*)-Benzylamine

structure	ΔG_{DMSO}	structure	ΔG_{DMSO}
$Pd_3(OAc)_6$	0	$Pd_3(OAc)_6$	0
S$_{5B}$	−2.6	**S$_{5C}$**	−1.6
TS$_{S3B}$	39.5	**TS$_{S3C}$**	41.8
S$_{6B}$	−3.0	**S$_{6C}$**	−1.9

Table 5. Relative Gibbs Free Energy (ΔG_{DMSO}, in kcal/mol) in Figures S34, S36, and S38 in the Supporting Information for Generation of the (*S*)-Iodinated Product and the Regeneration of the Catalyst

structure	ΔG_{DMSO}	structure	ΔG_{DMSO}	structure	ΔG_{DMSO}
$Pd_3(OAc)_6$	0	$Pd_3(OAc)_6$	0	$Pd_3(OAc)_6$	0
S$_{8A}$	−1.8	**S$_{8B}$**	4.6	**S$_{8C}$**	5.6
TS$_{S5A}$	−1.3	**TS$_{S5B}$**	5.8	**TS$_{S5C}$**	10.3
S$_{9A}$	−3.7	**R$_{S9B}$**	−1.6	**R$_{S9C}$**	1.4
HI	6.0	**10**	−9.9	HI	6.0
		TS$_6$	1.5		
		11	−9.6		
		HI	6.0		

out the calculations and find it is true that DMSO can also facilitate the C−H activation through a space effect. Our calculation shows that the C−H activation transition state with DMSO (**TS$_{R2a\text{-}DMSO}$**) has stability similar to that of the transition state with acetic acid (**TS$_{R2a}$**) in the gas phase but **TS$_{R2a\text{-}DMSO}$** is more stable than **TS$_{R2a}$** after solvent correction, the same as for (*S*)-benzylamine (Scheme 3). Here, we need to clarify that the stability of **TS$_{R2a\text{-}DMSO}$** in the solution phase is in contrast to the experimental result that C−H activation was the rate-determining step. Therefore, the solvent correction to **TS$_{R2a\text{-}DMSO}$** may be overestimated but the effect of DMSO is definitely positive. However, in the unfavorable transition states (**TS$_{R2a'}$** and **TS$_{S2A'}$**) the MPAA ligand is flexible and weakly coordinates to the Pd center due to a trans effect from the N−Pd bond, making the proton transfer from the phenyl group to the carboxylate group of the MPAA ligand difficult.

The highest selectivity (rate of fast-reacting enantiomer/rate of slow-reacting enantiomer) of the kinetic resolution in the experiment is 244, showing that the activation barrier difference between the (*R*)-benzylamine and (*S*)-benzylamine is about 3.7 kcal/mol. However, the calculated reaction barrier difference between these two enantiomers is 7.3 kcal/mol, which is consistent with the experimental results, expect for the 3.6 kcal/mol error, which may come from the model substrate and ligand used in the calculations.

In order to investigate the important role of the directing group SO_2CF_3 (Tf) in *R* and *S* substrates, Tf has been replaced with CH_3 when calculating the energy changes in C−H bond cleavage processes (Figures S40 and S41 in the Supporting Information). **TS$_{2R\text{-}Me}$** is calculated to be 9.0 kcal/mol higher in energy than **TS$_{R2a}$** and lower in energy than **TS$_{2S\text{-}Me}$** by 4.9 kcal/mol (Table 6). These results may come from the strong electron withdrawing ability of Tf, which makes the deprotonation of amine group in substrate easy to occur. At the same time, the TfN−Pd bond is stronger than the MeN−Pd bond because TfN is a softer ligand than MeN, thus

DOI: 10.1021/acs.joc.5b02571
J. Org. Chem. 2016, 81, 1006−1020

Scheme 3. Most Stable Transition States for Ortho C−H Activation of (*R*)- and (*S*)-Benzylamine

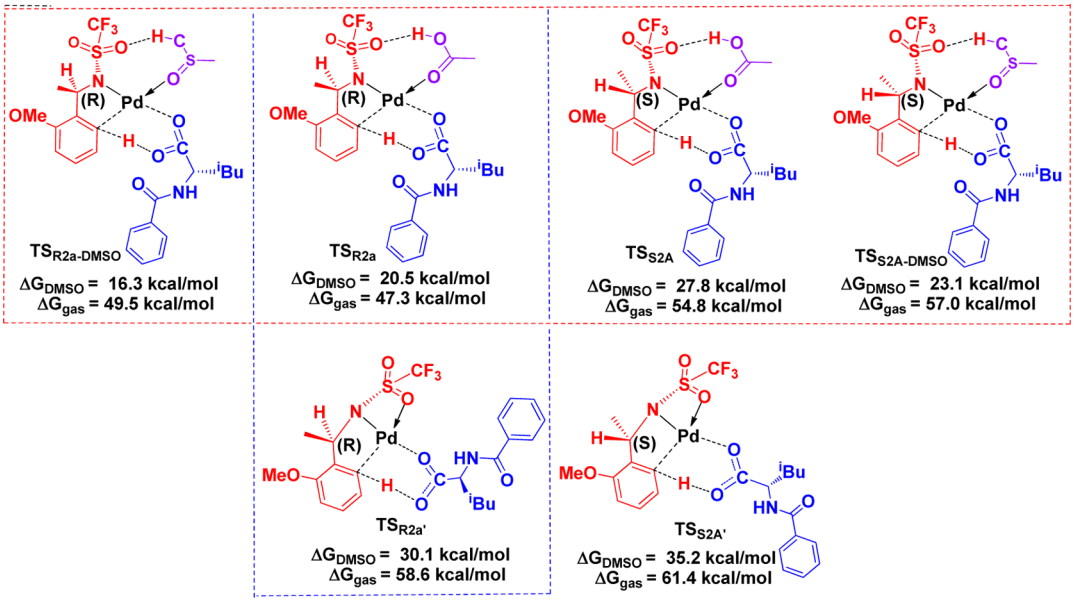

Table 6. Relative Gibbs Free Energy (ΔG_{DMSO}, in kcal/mol) in the DMSO of Pathways *R*-Me and *S*-Me in Figure S40 in the Supporting Information for Aryl C−H Bond Activation of Benzylamine

structure	ΔG_{DMSO}	structure	ΔG_{DMSO}
$Pd_3(OAc)_6$	0	$Pd_3(OAc)_6$	0
R-Me$_3$	9.3	**S-Me$_3$**	16.5
TS$_{2R-Me}$	29.5	**TS$_{2S-Me}$**	34.4
R-Me$_4$	17.7	**S-Me$_4$**	23.4

Scheme 4. Most Stable Transition States for Ortho C−H Activation of S_R-, S_S-, MeNH−C(*R*)-, and MeNH−C(*S*)-Substituted Benzene

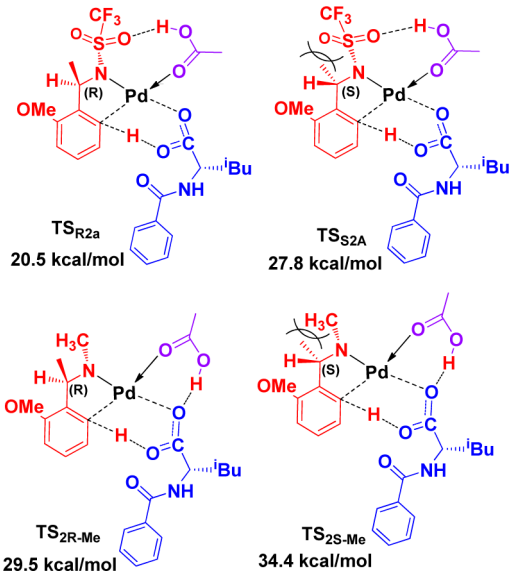

bringing the ortho C−H bond closer to the carboxylate of the MPAA ligand and making it more readily cleaved.

The calculated results for MeNH−C(*R*) and MeNH−C(*S*) confirmed that aryl C−H bond activation in (*R*)-benzylamine is more favorable than that in (*S*)-benzylamine. After comparison of the geometries of these C−H bond activation transition states, we found that the repulsion between the Me group on the chiral carbon and the Tf or Me group on the adjacent N atom is more obvious in (*S*)-benzylamine than that in (*R*)-benzylamine. It is this repulsion that makes **TS$_{2SA}$** and **TS$_{2S-Me}$** more unstable than **TS$_{2Ra}$** and **TS$_{2R-Me}$**, respectively (Scheme 4).

CONCLUSION

In this work, almost all possible reaction pathways for Pd-catalyzed enantioselective C−H iodination at room temperature have been investigated with DFT calculations. Our calculated results for ortho C−H iodation are collected in Scheme 5, which shows a schematic presentation of the most favorable pathways for both *R* and *S* enantiomers as reagents. Other aryl C−H bonds are more difficult to iodinate than the ortho C−H bond. In general, the palladium-mediated ortho C−H iodination reaction of (*R*)-benzylamines is carried out through three steps, namely: (1) *ortho* C−H bond activation, (2) oxidative addition and reductive elimination, and (3) regeneration of the catalyst. In the most favorable pathway, ortho C−H bond activation via nucleophilic attack of basic MPAA carboxylate is the rate-determining step for both (*R*)- and (*S*)-benzylamine, where acetic acid or DMSO coordination on the metal center makes the space economy sufficient and squeezes the ortho C−H of the substrate closer to the carboxylate group of the MPAA ligand to cause proton transfer. However, the favorable Pd−N(substrate) bond formation defines that ortho C−H is more preferably activated by the Pd center than other aryl C−H bonds. It is worth mentioning that the Tf group at the amine group of the substrate leads to the formation of a strong Pd−N(substrate) bond, making the ortho C−H bond easily activated by the Pd center and carboxylate group of the MPAA ligand. After that, the formation of a C−I bond goes through I_2 oxidative addition and reductive elimination of the C−I bond, rather than a metathesis of the Pd−C bond with I_2. Last but not least, the catalytic cycle is finished by adding base to neutralize the byproduct HI. Importantly, the energy barriers of these three steps for (*R*)-benzylamine are all lower than those for (*S*)-

DOI: 10.1021/acs.joc.5b02571
J. Org. Chem. 2016, 81, 1006−1020

Scheme 5. Schematic Presentation of Major Mechanistic Steps of (*R*)-/(*S*)-Benzylamine Iodination

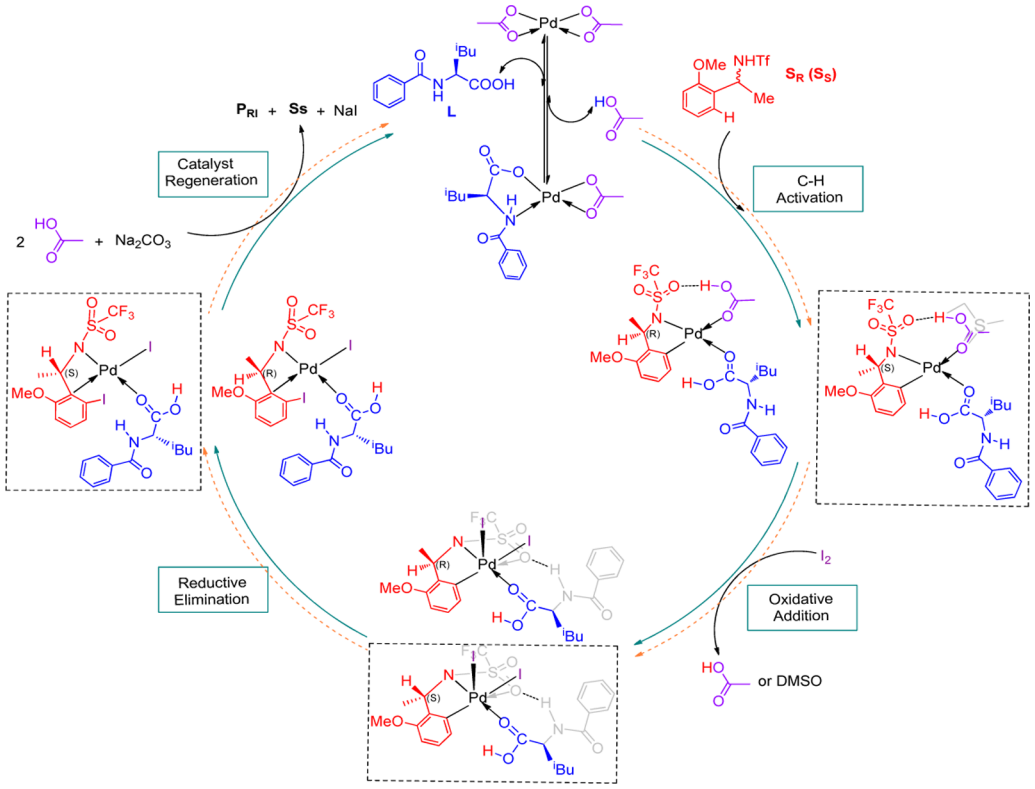

benzylamine, which is consistent with the experimental results that (*R*)-benzylamine was iodinated more quickly.

■ ASSOCIATED CONTENT

Supporting Information

The Supporting Information is available free of charge on the ACS Publications website at DOI: 10.1021/acs.joc.5b02571.

Structures of optimized compounds/intermediates and transition states, unfavorable pathways, Cartesian coordinates and electronic energies for all of the calculated structures, and energies in the gas phase and solution phase (PDF)

■ AUTHOR INFORMATION

Corresponding Author

*E-mail for L.D.: dangl@sustc.edu.cn.

Notes

The authors declare no competing financial interest.

■ ACKNOWLEDGMENTS

Financial support was obtained from Shenzhen special funds for the development of new energy (No. JCYJ20140714151402764) and the National Natural Science Foundation of China (No. 21573102), L.D. is grateful to the South University of Science and Technology of China.

■ REFERENCES

(1) (a) Giri, R.; Shi, B. F.; Engle, K. M.; Maugel, N.; Yu, J.-Q. *Chem. Soc. Rev.* **2009**, *38*, 3242−3272. (b) Ye, B.; Cramer, N. *Acc. Chem. Res.* **2015**, *48*, 1308−1318. (c) Wang, P. S.; Liu, P.; Zhai, Y. J.; Lin, H. C.; Han, Z. Y.; Gong, L. Z. *J. Am. Chem. Soc.* **2015**, *137*, 12732−12735. (d) Laforteza, B. N.; Chan, K. S. L; Yu, J. Q. *Angew. Chem., Int. Ed.* **2015**, *54*, 11143−11146.

(2) (a) Chen, X.; Engle, K. M.; Wang, D. H.; Yu, J.-Q. *Angew. Chem., Int. Ed.* **2009**, *48*, 5094−5115. (b) Lyons, T. W.; Sanford, M. S. *Chem. Rev.* **2010**, *110*, 1147−1169. (c) Shi, B. F.; Zhang, Y. H.; Lam, J. K.; Wang, D. H.; Yu, J.-Q. *J. Am. Chem. Soc.* **2010**, *132*, 460−461. (d) Musaev, D. G.; Kaledin, A.; Shi, B.-F.; Yu, J.-Q. *J. Am. Chem. Soc.* **2012**, *134*, 1690−1698. (e) Gao, D.-W.; Shi, Y.-C.; Gu, Q.; Zhao, Z.-L.; You, S.-L. *J. Am. Chem. Soc.* **2013**, *135*, 86−89.

(3) (a) Wasa, M.; Engle, K. M.; Lin, D. W.; Yoo, E. J.; Yu, J.-Q. *J. Am. Chem. Soc.* **2011**, *133*, 19598−19601. (b) Cheng, X.-F.; Li, Y.; Su, Y.-M.; Yin, F.; Wang, J.-Y.; Sheng, J.; Vora, H. U.; Wang, X.-S.; Yu, J.-Q. *J. Am. Chem. Soc.* **2013**, *135*, 1236−1239.

(4) (a) Micskei, K.; Patonay, T.; Caglioti, L.; Pályi, G. *Chem. Biodiversity* **2010**, *7*, 1660−1669. (b) Woodward, S.; Diéguez, M.; Pàmies, O. *Coord. Chem. Rev.* **2010**, *254*, 2007−2030. (c) Haines, B. E.; Musaev, D. G. *ACS Catal.* **2015**, *5*, 830−840.

(5) (a) Engle, K. M.; Thuy-Boun, P. S.; Dang, M.; Yu, J.-Q. *J. Am. Chem. Soc.* **2011**, *133*, 18183−18193. (b) Engle, K. M.; Yu, J.-Q. *J. Org. Chem.* **2013**, *78*, 8927−8955. (c) Li, G.; Leow, D.; Wan, L.; Yu, J.-Q. *Angew. Chem., Int. Ed.* **2013**, *52*, 1245−1247.

(6) (a) Shi, B.-F.; Maugel, N.; Zhang, Y.-H.; Yu, J.-Q. *Angew. Chem., Int. Ed.* **2008**, *47*, 4882−4886. (b) Chu, L.; Wang, X.-C.; Moore, C. E.; Rheingold, A. L.; Yu, J.-Q. *J. Am. Chem. Soc.* **2013**, *135*, 16344−16347. (c) Wan, L.; Dastbaravardeh, N.; Li, G.; Yu, J.-Q. *J. Am. Chem. Soc.* **2013**, *135*, 18056−18059. (d) Wang, X.-C.; Gong, W.; Fang, L.-Z.; Zhu, R.-Y.; Li, S.; Engle, K. M.; Yu, J.-Q. *Nature* **2015**, *519*, 334−338. (e) Dong, Z.; Wang, J.; Dong, G. *J. Am. Chem. Soc.* **2015**, *137*, 5887−5890.

(7) (a) Huang, C.; Chattopadhyay, B.; Gevorgyan, V. *J. Am. Chem. Soc.* **2011**, *133*, 12406−12409. (b) Novák, P.; Correa, A.; Gallardo-Donaire, J.; Martin, R. *Angew. Chem., Int. Ed.* **2011**, *50*, 12236−12239. (c) Wang, Y.-N.; Guo, X.-Q.; Zhu, X.-H.; Zhong, R.; Cai, L.-H.; Hou, X.-F. *Chem. Commun.* **2012**, *48*, 10437−10439. (d) Cong, X.; You, J.; Gao, G.; Lan, J. *Chem. Commun.* **2013**, *49*, 662−664.

(8) (a) Li, Y.; Ding, Y.-J.; Wang, J.-Y.; Su, Y.-M.; Wang, X.-S. *Org. Lett.* **2013**, *15*, 2574−2577. (b) Wang, H.-L.; Hu, R.-B.; Zhang, H.; Zhou, A.-X.; Yang, S.-D. *Org. Lett.* **2013**, *15*, 5302−5305. (c) Pi, C.; Li, Y.; Cui, X.; Zhang, H.; Han, Y.; Wu, Y. *Chem. Sci.* **2013**, *4*, 2675−2679.

DOI: 10.1021/acs.joc.5b02571
J. Org. Chem. 2016, 81, 1006−1020

(d) Wen, Z.-K.; Xu, Y.-H.; Loh, T.-P. *Chem. Sci.* **2013**, *4*, 4520−4524. (e) Meng, X.; Kim, S. *J. Org. Chem.* **2013**, *78*, 11247−11254. (f) Lee, S.; Lee, H.; Tan, K. L. *J. Am. Chem. Soc.* **2013**, *135*, 18778−18781.
(9) (a) Yang, G.; Lindovska, P.; Zhu, D.; Kim, J.; Wang, P.; Tang, R. Y.; Movassaghi, M.; Yu, J. Q. *J. Am. Chem. Soc.* **2014**, *136*, 10807−10813. (b) Tang, R. Y.; Li, G.; Yu, J.-Q. *Nature* **2014**, *507*, 215−220. (c) Bera, M.; Maji, A.; Sahoo, S. K.; Maiti, D. *Angew. Chem., Int. Ed.* **2015**, *54*, 8515−8519.
(10) (a) Cho, J. Y.; Tse, M. K.; Holmes, D.; Maleczka, R. E.; Smith, M. R. *Science* **2002**, *295*, 305−308. (b) Ishiyama, T.; Takagi, J.; Ishida, K.; Miyaura, N.; Anastasi, N. R.; Hartwig, J. F. *J. Am. Chem. Soc.* **2002**, *124*, 390−391. (c) Phipps, R. J.; Gaunt, M. J. *Science* **2009**, *323*, 1593−1597. (d) Duong, H. A.; Gilligan, R. E.; Cooke, M. L.; Phipps, R. J.; Gaunt, M. J. *Angew. Chem., Int. Ed.* **2011**, *50*, 463−466. (e) Julia-Hernandez, F.; Simonetti, M.; Larrosa, I. *Angew. Chem., Int. Ed.* **2013**, *52*, 11458−11460.
(11) Leow, D.; Li, G.; Mei, T.-S.; Yu, J.-Q. *Nature* **2012**, *486*, 518−522.
(12) Cheng, G.-J.; Yang, Y.-F.; Liu, P.; Chen, P.; Sun, T.-Y.; Li, G.; Zhang, X.; Houk, K. N.; Yu, J.-Q.; Wu, Y.-D. *J. Am. Chem. Soc.* **2014**, *136*, 894−897.
(13) (a) Li, J.-J.; Mei, T.-S.; Yu, J.-Q. *Angew. Chem., Int. Ed.* **2008**, *47*, 6452−6456. (b) Wang, X.; Mei, T.-S.; Yu, J.-Q. *J. Am. Chem. Soc.* **2009**, *131*, 7520−7521. (c) Vickers, C.; Mei, T.-S.; Yu, J.-Q. *Org. Lett.* **2010**, *12*, 2511−2513.
(14) Chu, L.; Xiao, K.-J.; Yu, J.-Q. *Science* **2014**, *346*, 451−455.
(15) (a) Liu, P.; Yang, X.; Birman, V. B.; Houk, K. N. *Org. Lett.* **2012**, *14*, 3288−3291. (b) Qabaja, G.; Benavides, A. R.; Liu, S.; Petersen, K. S. *J. Org. Chem.* **2015**, *80*, 133−140. (c) Odagi, M.; Furukori, K.; Yamamoto, Y.; Sato, M.; Iida, K.; Yamanaka, M.; Nagasawa, K. *J. Am. Chem. Soc.* **2015**, *137*, 1909−1915.
(16) Cheng, G.-J.; Chen, P.; Sun, T.-Y.; Zhang, X.; Yu, J.-Q.; Wu, Y.-D. *Chem. - Eur. J.* **2015**, *21*, 11180−11188.
(17) (a) Becke, A. D. *J. Chem. Phys.* **1993**, *98*, 1372. (b) Lee, C.; Yang, W.; Parr, R. G. *Phys. Rev. B: Condens. Matter Mater. Phys.* **1988**, *37*, 785.
(18) Frisch, M. J.; Trucks, G. W.; Schlegel, H. B.; Scuseria, G. E.; Robb, M. A.; Cheeseman, J. R.; Scalmani, G.; Barone, V.; Mennucci, B.; Petersson, G. A.; Nakatsuji, H.; Caricato, M.; Li, X.; Hratchian, H. P.; Izmaylov, A. F.; Bloino, J.; Zheng, G.; Sonnenberg, J. L.; Hada, M.; Ehara, M.; Toyota, K.; Fukuda, R.; Hasegawa, J.; Ishida, M.; Nakajima, T.; Honda, Y.; Kitao, O.; Nakai, H.; Vreven, T.; Montgomery, J. A., Jr.; Peralta, J. E.; Ogliaro, F.; Bearpark, M.; Heyd, J. J.; Brothers, E.; Kudin, K. N.; Staroverov, V. N.; Kobayashi, R.; Normand, J.; Raghavachari, K.; Rendell, A.; Burant, J. C.; Iyengar, S. S.; Tomasi, J.; Cossi, M.; Rega, N.; Millam, J. M.; Klene, M.; Knox, J. E.; Cross, J. B.; Bakken, V.; Adamo, C.; Jaramillo, J.; Gomperts, R.; Stratmann, R. E.; Yazyev, O.; Austin, A. J.; Cammi, R.; Pomelli, C.; Ochterski, J. W.; Martin, R. L.; Morokuma, K.; Zakrzewski, V. G.; Voth, G. A.; Salvador, P.; Dannenberg, J. J.; Dapprich, S.; Daniels, A. D.; Farkas, Ö.; Foresman, J. B.; Ortiz, J. V.; Cioslowski, J.; Fox, D. J. *Gaussian 09, Revision D.01*; Gaussian, Inc., Wallingford, CT, 2009.
(19) (a) Zhao, Y.; Truhlar, D. G. *Theor. Chem. Acc.* **2008**, *120*, 215−241. (b) Zhao, Y.; Truhlar, D. G. *Acc. Chem. Res.* **2008**, *41*, 157−167.
(20) Cances, E.; Mennucci, B.; Tomasi, J. *J. Chem. Phys.* **1997**, *107*, 3032−3041.
(21) Chai, J. D.; Head-Gordon, M. *Phys. Chem. Chem. Phys.* **2008**, *10*, 6615−6620.
(22) (a) Tao, J.; Perdew, J. P.; Staroverov, V. N.; Scuseria, G. E. *Phys. Rev. Lett.* **2003**, *91*, 146401. (b) Staroverov, V. N.; Scuseria, G. E.; Tao, J.; Perdew, J. P. *J. Chem. Phys.* **2003**, *119*, 12129.
(23) (a) Gonzalez, C. H.; Schlegel, B. *J. Chem. Phys.* **1989**, *90*, 2154−2161. (b) Gonzalez, C.; Schlegel, H. B. *J. Phys. Chem.* **1990**, *94*, 5523−5527.
(24) (a) Bennett, M. A.; Milner, D. L. *J. Am. Chem. Soc.* **1969**, *91*, 6983−6994. (b) Ibers, J. A.; Dicosimo, R.; Whitesides, G. M. *Organometallics* **1982**, *1*, 13−20.

DOI: 10.1021/acs.joc.5b02571
J. Org. Chem. 2016, 81, 1006−1020